

This is an Open Access document downloaded from ORCA, Cardiff University's institutional repository: <https://orca.cardiff.ac.uk/id/eprint/89174/>

This is the author's version of a work that was submitted to / accepted for publication.

Citation for final published version:

Clark, Christopher Jonathan Redfern, Schofield, Simon, Gomez, Haley Louise and Davies, Jonathan Ivor 2016. An empirical determination of the dust mass absorption coefficient, κ_d , using the Herschel Reference Survey. Monthly Notices of the Royal Astronomical Society 459 (2) , pp. 1646-1658. 10.1093/mnras/stw647

Publishers page: <http://dx.doi.org/10.1093/mnras/stw647>

Please note:

Changes made as a result of publishing processes such as copy-editing, formatting and page numbers may not be reflected in this version. For the definitive version of this publication, please refer to the published source. You are advised to consult the publisher's version if you wish to cite this paper.

This version is being made available in accordance with publisher policies. See <http://orca.cf.ac.uk/policies.html> for usage policies. Copyright and moral rights for publications made available in ORCA are retained by the copyright holders.



An Empirical Determination of the Dust Mass Absorption Coefficient, κ_d , Using the Herschel Reference Survey

Christopher J. R. Clark^{1*}, Simon P. Schofield¹, Haley L. Gomez¹, Jonathan I. Davies¹

¹ *School of Physics & Astronomy, Cardiff University, Queens Buildings, The Parade, Cardiff, CF24 3AA, UK*

* *Christopher.Clark@astro.cf.ac.uk*

Accepted for publication in Monthly Notices of the Royal Astronomical Society

ABSTRACT

We use the published photometry and spectroscopy of 22 galaxies in the *Herschel* Reference Survey to determine that the value of the dust mass absorption coefficient κ_d at a wavelength of $500\ \mu\text{m}$ is $\kappa_{500} = 0.051^{+0.070}_{-0.026}\text{ m}^2\text{ kg}^{-1}$. We do so by taking advantage of the fact that the dust-to-metals ratio in the interstellar medium of galaxies appears to be constant. We argue that our value for κ_d supersedes that of [James et al. \(2002\)](#) – who pioneered this approach for determining κ_d – because we take advantage of superior data, and account for a number of significant systematic effects that they did not consider. We comprehensively incorporate all methodological and observational contributions to establish the uncertainty on our value, which represents a marked improvement on the oft-quoted ‘order-of-magnitude’ uncertainty on κ_d . We find no evidence that the value of κ_d differs significantly between galaxies, or that it correlates with any other measured or derived galaxy properties. We note, however, that the availability of data limits our sample to relatively massive ($10^{9.7} < M_\star < 10^{11.0}\text{ M}_\odot$), high metallicity ($8.61 < [12 + \log_{10} \frac{O}{H}] < 8.86$) galaxies; future work will allow us to investigate a wider range of systems.

Key words: galaxies: ISM – submillimetre: galaxies – submillimetre: ISM – ISM: dust – radio lines: ISM – galaxies: abundances

1 INTRODUCTION

The study of cosmic dust has advanced enormously over the past 10–15 years, with the advent of telescopes such as *Spitzer* ([Werner et al., 2004](#)), *Herschel* ([Pilbratt et al., 2010](#)), *Planck* ([Planck Collaboration et al., 2011](#)) and ALMA (the Atacama Large Millimetre/submillimetre Array). Observations of dust emission in the Far-InfraRed (FIR) and submillimetre (submm) now serve as some of our most potent tools for understanding the InterStellar Medium (ISM), providing us with avenues to investigate galaxies’ chemical evolution, star-formation, and interstellar environments.

However, our ability to use FIR and submm observations to *actually measure the mass of dust* in galaxies is notoriously limited. The dust mass absorption coefficient, κ_d (sometimes called the dust mass opacity coefficient), describes what mass of dust gives rise to an observed dust luminosity. However, the value of κ_d is very poorly constrained, leading to correspondingly large uncertainty on derived dust mass values. The value of κ_d is dictated by the physical properties of the dust, such as the mass density of the constituent materials, the efficiency with which they

emit, the grain surface-to-volume ratio, and the grain size distribution.

A wide range of values of κ_d have been estimated, using a variety of techniques. Most require making assumptions about the physical properties of dust grains. The raw materials that make up dust are actually quite well known; the majority of the mass of dust consists of C, N O, Mg, Si, and Fe. This is inferred from observations of the gas phase of the ISM, which is found to be highly depleted of these elements ([Savage & Sembach, 1996](#); [Jenkins, 2009](#)). Similarly, some information about the grain size distribution can be extracted from the UltraViolet (UV) dust extinction curve ([Kim et al., 1994](#); [Jones et al., 1996](#); [Gall et al., 2014](#)). Hence chemical considerations can be used to model the mineralogical and physical properties of dust ([Whittet, 1992](#); [Jones, 2013](#)). Numerous such models exist (eg, [Hildebrand, 1983](#); [Draine & Lee, 1984](#); [Draine & Li, 2007](#); [Jones et al., 2013](#)), and each implies a corresponding value of κ_d ; but there is a great deal of variation between the characteristics of the dust in these various models. Comparisons of FIR/submm emission and UV/optical extinction in Galactic nebulae can be used to estimate κ_d ([Casey, 1991](#); [Bianchi et al., 2003](#)),

but require assumptions about the cloud geometry, and the results may not apply beyond the nebulae in question, given the known variation of dust properties with environment (Cardelli et al., 1996; Smith et al., 2012b; Planck Collaboration et al., 2014a,b). A similar approach can be taken with entire nearby galaxies (Alton et al., 2000, 2004; Dasyra et al., 2005), but this likewise requires assumptions about the geometry and radiative transfer properties of the dust, in order to constrain the optical depth. Laboratory examination of dust analogues, informed by the composition of pre-solar dust grains, provides an alternate approach for determining κ_d (Mutschke, 2013; Demyk et al., 2013). However only a small number of truly pre-solar dust grains have been retrieved for analysis (Messenger et al., 2013), so it is hard to establish the relative importance in the bulk composition of interstellar dust of the particular materials being studied in the laboratory.

The values of κ_d suggested by these methods vary enormously. See the summary tables in Alton et al. (2004) and Demyk et al. (2013) for a range of observationally- and experimentally-derived values. We can compare values of κ_d determined at different wavelengths using the relation:

$$\kappa_\lambda = \kappa_0 \left(\frac{\lambda_0}{\lambda} \right)^\beta \quad (1)$$

where κ_λ is the value of κ_d at some wavelength λ , κ_0 is the reference value of κ_d at some reference wavelength λ_0 , and β is the dust emissivity spectral index.

The literature values of κ_d listed in the summary tables of Alton et al. (2004) and Demyk et al. (2013), along with several other commonly-cited values (Draine, 2003; Dasyra et al., 2005; Draine & Li, 2007; Eales et al., 2010; Compiègne et al., 2011), are plotted in Figure 1, converted¹ to κ_{500} as per Equation 1 (only using values where $\lambda_0 \geq 250 \mu\text{m}$, and assuming $\beta = 2$ as a basic approximation). These 46 values have a standard deviation of 0.8 dex, and span over 3.5 orders of magnitude in total, ranging from $\kappa_{500} = 0.031 \text{ m}^2 \text{ kg}^{-1}$ to $\kappa_{500} = 104 \text{ m}^2 \text{ kg}^{-1}$.

This vast uncertainty in κ_d is extremely troubling, especially considering that the observed dust mass of a galaxy is now being used as a proxy for estimating other quantities, such as the total gas mass (Eales et al., 2012; Scoville et al., 2014). Modulo the uncertainty on the value of κ_d , this promises to be a useful tool, particularly at high redshift where other gas estimators may not be available.

Ideally, in order to calibrate a robust value for κ_d , there would be a way to *a priori* know the dust mass present in a galaxy, without reference to FIR/submm observations. Fortunately, James et al. (2002) demonstrated that this is, in fact, possible. It has been 13 years since James et al. first applied their technique; with the advent of *Herschel*, and the greatly improved quality of extragalactic observations now available, the time is now ripe to repeat their analysis, taking advantage of the the greatly improved resources at our disposal.

In Section 2 we describe the James et al. method, and

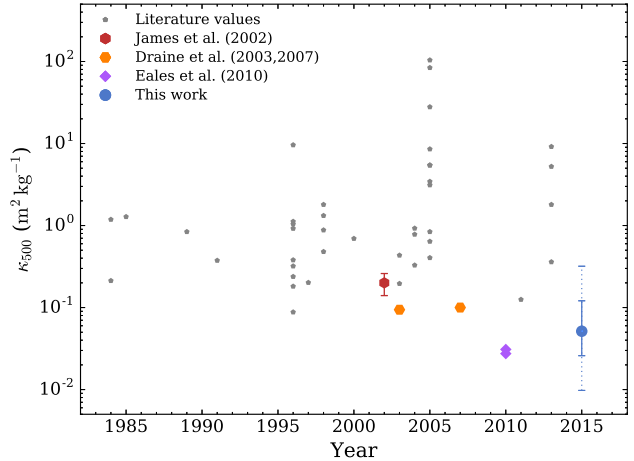


Figure 1. Literature values of κ_{500} , taken from the summary tables of Alton et al. (2004) and Demyk et al. (2013), along with several other widely-cited values (Draine, 2003; Dasyra et al., 2005; Draine & Li, 2007; Eales et al., 2010; Compiègne et al., 2011), plotted against their year of publication. There is no indication that reported values of κ_d are converging as time goes by. Highlighted is the value of κ_d found by James et al., whose method this work is based upon; Eales et al. (2010), who used a resolved variant of the James et al. method for two galaxies; and the very commonly-used values of Draine (2003) and Draine & Li (2007). Also shown for later comparison is the value of κ_d we determine in Section 5. The solid error bar shows the uncertainty derived in Section 5.1, whilst the dotted error bar indicates the potential extent of the systematic offset due to the fact that the absolute metallicity scale calibration is not known to better than 0.7 dex (Kewley & Ellison, 2008, see Section 2). Note that some of the scatter in this plot will be due to differences in the metallicity prescriptions employed; we opt not to correct for this, therefore keeping the plot representative of the *absolute* variation in reported values of κ_d .

how we intend to apply it. In Section 3 we outline the *Herschel* Reference Survey, the sample we use to perform our analysis. In Section 4 we describe how we fit the dust SEDs of the galaxies in our sample. In Section 5 we put the method into practice, to arrive at a new, well-constrained value for κ_d . In Section 6 we look at how our computed values for κ_d vary across our sample. In Section 7 we compare our value for κ_d to other reported values.

2 THE METHOD

The James et al. method for determining the value of κ_d takes advantage of the fact that the fraction of the metals in a galaxy's ISM that are locked up in dust, ε_d , appears to be constant. A wealth of evidence supports the notion that ε_d is constant in the modern universe (Sodroski et al., 1997; Dwek, 1998; Leroy et al., 2011; Watson, 2011; Smith et al., 2012a; Corbelli et al., 2012), with further work suggesting it is also constant at high redshift (Pei, 1992; Pei et al., 1999; Zafar & Watson, 2013; Chen et al., 2013; Sparre et al., 2014). There also exist theoretical frameworks to explain the observed invariance in ε_d (Inoue, 2003; Asano et al., 2011; Mattsson et al., 2014). It should however be noted that there is conflict in the literature on the matter of whether or not

¹ Where the Demyk et al. (2013) summary table states a κ_d that depends upon temperature, with entries for both 300 K and 10 K, the 10 K value has been taken.

ε_d remains constant in low-metallicity systems; some studies find that ε_d differs in low-metallicity dwarf galaxies (Galilano et al., 2005; Hunt et al., 2005), whereas others have found ε_d to be constant over a wide range of masses, metallicities, and redshifts (Pei, 1992; Zafar & Watson, 2013).

Many of the interstellar dust-to-metals ratios quoted in the literature are not suitable for the purposes of this work. Some quote the dust-to-metals ratio in terms of extinction per column density of metals, A_V/N_{H_X} (eg, Watson, 2011; Zafar & Watson, 2013; Sparre et al., 2014), which cannot be converted to a value of ε_d without assuming what column density of dust corresponds to a given degree of extinction – and given that the aim of this work is to determine the dust mass-to-emission ratio, it would be unwise to predicate it upon assumptions about the equally poorly-constrained dust mass-to-extinction ratio. There are also works which use an assumed value of κ_d to arrive at their value for ε_d (eg, Smith et al., 2012a; Davies et al., 2014); as such, any attempt to use these values to estimate κ_d would be an exercise in circular logic.

Fortunately, there are numerous values of ε_d reported in the literature which are suitable for the purposes of determining κ_d , from studies which examine elemental depletions to establish the fraction of metals locked up in dust grains. The values we consider are 0.5 (Issa et al., 1990), 0.36 (Luck & Lambert, 1992, Large Magellanic Cloud), 0.46 (Luck & Lambert, 1992, Small Magellanic Cloud), 0.5 (Whittet, 1992), 0.51 (Pei, 1992), 0.36 (Meyer et al., 1998), 0.3 (Dwek, 1998), 0.45 (Pei et al., 1999), 0.529 (Weingartner & Draine, 2001), 0.456 (James et al., 2002), 0.549 (Kimura et al., 2003), and 0.387 (Draine et al., 2007). The average (mean, median, and mode) of these 12 values is 0.5, and the standard deviation is 0.1; hence we adopt a value for the interstellar dust-to-metals ratio of $\varepsilon_d = 0.5 \pm 0.1$.

Using ε_d requires knowledge of the metallicity of a galaxy’s ISM. Gas-phase metallicity is generally expressed in terms of the logarithm of the oxygen-to-hydrogen bulk abundance ratio, in the form $[12 + \log_{10} \frac{O}{H}]$; in such units, the Solar metallicity is 8.69 ± 0.05 (Asplund et al., 2009). Because we are concerned with the absolute metal mass fraction, we convert $[12 + \log_{10} \frac{O}{H}]$ metallicities to metal mass fractions by reference to the Solar values; we use a Solar metal mass fraction of $f_{Z_\odot} = 0.0134$ (Asplund et al., 2009², uncertainty assumed to be negligible). This does entail the assumption that $[12 + \log_{10} \frac{O}{H}]$ metallicity is a direct proxy for absolute metallicity. A wide variety of combinations of atomic species and emission lines are commonly used to estimate $[12 + \log_{10} \frac{O}{H}]$ metallicity (OII, OIII, NII, SII H α , H β , etc); Kewley & Ellison (2008) have shown how different metallicity prescriptions can be normalised to give $[12 + \log_{10} \frac{O}{H}]$ values with a relative accuracy of < 0.1 dex, but that the *absolute* metallicity scale calibration is not known to better than 0.7 dex. The represents a systematic uncertainty on any absolute metallicity, including those we use here. Because it is a systematic, we do not incorporate it into our uncertainty analysis in Section 5.1; rather, we stress to the reader that there is some underlying fixed offset between the metal

mass fractions we (and any other authors) employ, and the corresponding true metal mass fractions, of up to 0.7 dex.

It is also important to note that $[12 + \log_{10} \frac{O}{H}]$ is a tracer of *gas-phase* metallicity – whereas we are interested in the metallicity of the entire ISM. When using gas-phase oxygen abundance to determine ISM metallicity, a correction needs to be applied to account for the fraction of oxygen depleted onto dust grains. Specifically, this correction needs to account for the oxygen depletion level in HII regions, which are the source of the majority of the nebular line emission of star-forming galaxies (Kunth & Östlin, 2000), and hence are where empirical gas-phase metallicity estimators are calibrated (including those used in this work, see Section 3). We perform this correction using the Mesa-Delgado et al. (2009) oxygen-depletion factor of $\delta_O = 1.32 \pm 0.09$, determined by observing reductions in oxygen depletion due to dust destruction in shocked regions of Orion Nebula. This value is in good agreement with the values of δ_O reported by Zurita & Bresolin (2012) from comparisons of HII regions and blue supergiants in M31, Patterson et al. (2012) and Kudritzki et al. (2012) for M81, and Peimbert & Peimbert (2010) for galactic HII regions. It should be noted that studies suggests δ_O decreases in low-metallicity environments, with no depletion observed by Bresolin et al. (2009) in NGC 0300 ($[12 + \log_{10} \frac{O}{H}] \sim 8.3$), and $\delta_O = 1.20$ found by Peimbert & Peimbert (2010) in low-metallicity galaxy SBS 0335-052 E ($[12 + \log_{10} \frac{O}{H}] \sim 7.4$). However, as all of the galaxies we consider in this work have at least double these metallicities ($[12 + \log_{10} \frac{O}{H}] > 8.61$, see Section 3), the value of δ_O we adopt should be unaffected.

Assuming that ε_d is indeed constant, the dust mass M_d in a galaxy will be given by:

$$M_d = M_g \varepsilon_d f_{Z_\odot} Z \quad (2)$$

where M_g is the gas mass of a galaxy’s ISM, f_{Z_\odot} is the metal mass fraction at Solar metallicity, and Z is the metallicity of a galaxy’s ISM as a fraction of the Solar value.

The value of Z for the galaxy in question is arrived at using its $[\frac{O}{H}]$ bulk abundance ratio measurement (converted from $[12 + \log_{10} \frac{O}{H}]$ format), corrected for gas-phase oxygen depletion, according to:

$$Z = \delta_O \left[\frac{O}{H} \right] / \left[\frac{O}{H} \right]_\odot \quad (3)$$

where $[\frac{O}{H}]_\odot$ is the Solar oxygen bulk abundance ratio.

The total mass of a galaxy’s ISM is:

$$M_g = \xi (M_{HI} + M_{H_2}) \quad (4)$$

where M_{HI} is the mass of atomic hydrogen, M_{H_2} is the mass of molecular hydrogen, and ξ is a correction factor to account for the fraction of a galaxy’s ISM made up of elements heavier than hydrogen, defined as:

$$\xi = \frac{1}{1 - \left(f_{He_p} + f_Z \left[\frac{\Delta f_{He}}{\Delta f_Z} \right] \right) - f_Z} \quad (5)$$

where f_{He_p} is the primordial helium mass fraction of 0.2485 ± 0.0002 (Aver et al., 2013), f_Z is the metal mass fraction of

² We note that this value for the Solar metal mass fraction is ~ 33 percent lower than values typically used pre-2005 (see Asplund et al., 2009).

the galaxy in question (such that $f_Z = f_{Z_\odot} Z$), and $[\frac{\Delta f_{He}}{\Delta f_Z}]$ is the evolution of the helium mass fraction with metallicity (such that the helium mass fraction $f_{He} = f_{He_p} + f_Z [\frac{\Delta f_{He}}{\Delta f_Z}]$) for which we use a rate of $[\frac{\Delta f_{He}}{\Delta f_Z}] = 1.41 \pm 0.62$ (Balser, 2006). In the literature, it is common to account for helium alone, and assume solar metallicity when doing so, equivalent to using a correction factor of $\xi = 1.36$. However, this ignores the mass contribution of metals, and the fact that the helium fraction is metallicity-dependant; a galaxy with zero metallicity would have $\xi = 1.33$, whilst $\xi = 1.39$ at solar metallicity.

The mass of atomic hydrogen (in Solar masses) in a galaxy is determined from 21 cm observations using the standard prescription:

$$M_{HI} = 2.356 \times 10^5 S_{HI} D^2 \quad (6)$$

where S_{HI} is the integrated 21 cm line flux density in Jy km s^{-1} , and D is the source distance in Mpc.

The mass of molecular hydrogen in a galaxy (in Solar masses) is typically inferred from the luminosity of the $^{12}\text{C}^{16}\text{O}(1-0)$ line, according to:

$$M_{H_2} = 2.453 \times 10^3 S_{CO} D^2 \alpha_{CO} \quad (7)$$

where S_{CO} is the integrated flux density of the $^{12}\text{C}^{16}\text{O}(1-0)$ line in Jy km s^{-1} , D is the source distance in Mpc, and α_{CO} is the CO-to- H_2 conversion factor in $\text{M}_\odot \text{K}^{-1} \text{km}^{-1} \text{s}$. We opt to use the metallicity-dependant α_{CO} prescription of Schrubba et al. (2012), which takes the form:

$$\log_{10}(\alpha_{CO} \xi) = \log_{10}(A) + N \left(\left[12 + \log_{10} \frac{O}{H} \right] - 8.7 \right) \quad (8)$$

where A and N are empirical calibration constants determined by Schrubba et al. (2012) with values $A = 8.0 \pm 1.3$ and $N = -2.0 \pm 0.4$. Schrubba et al. (2012) calibrated this prescription empirically over a 1 dex range in metallicity ($8 < [12 + \log_{10} \frac{O}{H}] < 9$), encompassing the full metallicity range of the galaxies we consider in this work (see Section 3), and find 0.1 dex of scatter on the prescription as a whole. Note that for the metallicity range of the galaxies we consider in this work (see Section 3), the Schrubba et al. (2012) prescription is compatible with the alternative metallicity-dependant prescription of Genzel et al. (2012).

We include the ξ term in Equation 8 to account for the fact that the Schrubba et al. (2012) prescription is calibrated using the rate at which star-forming material is consumed, and hence includes the mass of helium (and other elements) associated with the molecular hydrogen being traced by the CO (A.K. Leroy, *priv. comm.*) – whereas we are only concerned with the mass of molecular hydrogen.

The FIR–submm ($50 < \lambda < 1000 \mu\text{m}$) emission from dust in a galaxy is described by a two-component modified blackbody Spectral Energy Distribution (SED), which takes the form:

$$M_d = \frac{S_{\lambda_w} D^2}{\kappa_\lambda B_\lambda(T_w)} + \frac{S_{\lambda_c} D^2}{\kappa_\lambda B_\lambda(T_c)} \quad (9)$$

where S_{λ_w} and S_{λ_c} are the flux densities of the warm and cold dust components at wavelength λ in $\text{W Hz}^{-1} \text{m}^{-2}$, and

$B_\lambda(T_w)$ and $B_\lambda(T_c)$ are each the Planck function at wavelength λ and characteristic dust temperatures T_w and T_c . Whilst a single-component modified blackbody would be a simpler model, recent work has shown that this approach can systematically fail to fit the SEDs of certain galaxies; we expand upon this, and detail how our SED fitting is performed, in Section 4.

Substituting Equation 4 into Equation 2, setting that equal to Equation 9, and re-arranging to make κ_λ the subject, gives us the formula:

$$\kappa_\lambda = \frac{D^2}{\xi (M_{HI} + M_{H_2}) \varepsilon_d f_{Z_\odot} Z} \left(\frac{S_{\lambda_w}}{B_\lambda(T_w)} + \frac{S_{\lambda_c}}{B_\lambda(T_c)} \right) \quad (10)$$

which can be used to empirically determine the value of κ_d for any galaxy for which FIR–submm photometry, atomic gas mass, molecular gas mass, and integrated gas-phase metallicity is available. Note that the resulting value of κ_d is not affected by uncertainty in source distance, because the terms for both M_{HI} and M_{H_2} are proportional to D^2 ; as such D^2 ultimately cancels out of Equation 10.

Whilst the method we have laid out here follows the same basic principle as that of James et al., we note that they did not explicitly account for the mass helium or metals when considering their ISM masses, whereas we do so by including the ξ term in Equation 4; the metallicities of the galaxies we consider in this work (see Section 3) give a median value of $\xi = 1.41$, and hence our ultimate value of κ_d will also be reduced by a factor of 1.41 (see Equation 10). Nor did the James et al. method appear to account for the depletion of oxygen onto dust, despite the fact that they used measurements of gas-phase oxygen abundance, pegged to Solar values, to determine absolute metallicities; given our adopted correction of $\delta_O = 1.32$, the factor by which our values of κ_d will be reduced as a result of this consideration will likewise be 1.32. Combined, ξ and δ_O will reduce any value of κ_d by a factor of 1.86 – our inclusion of these systematic effects hence represents an essential development of the James et al. technique.

3 THE SAMPLE

To perform our determination of κ_d , we use the rich, homogeneous dataset of the *Herschel* Reference Survey (HRS, Boselli et al., 2010). The HRS consists of 323 galaxies in the velocity range $1050 \leq V \leq 1750 \text{ km s}^{-1}$ (with corrections made to account for the velocity dispersion of the galaxies of the Virgo Cluster), corresponding to a distance range of $15 \leq D \leq 25 \text{ Mpc}$. The HRS galaxies were selected on the basis of their K_S -band brightness, as this is the part of the stellar emission spectrum that suffers least from extinction, and is known to be a good proxy for stellar mass. The apparent magnitude limit of the late type galaxies in HRS is $K_S \leq 12$, which equates to an absolute magnitude limit in the range $-17.43 \leq K_S \leq -18.54$, depending on the distance of the source between the HRS limits. For early type galaxies, a brighter apparent magnitude limit of $K_S \leq 8.7$ is applied.

The HRS has excellent multiwavelength photometric

data available. The *Herschel*-SPIRE³ photometry is presented in Ciesla et al. (2012), *Herschel*-PACS⁴ photometry in Cortese et al. (2014), WISE⁵ photometry in Ciesla et al. (2014), and SDSS⁶ and GALEX⁷ photometry in Cortese et al. (2012a) (note that not all of this photometry is used in our determination of κ_d ; the SDSS and GALEX data is used in Section 6, when comparing κ_d to other galaxy properties).

Drift-scan spectroscopy of the HRS galaxies is presented in Boselli et al. (2013); this data is in turn used by Hughes et al. (2013) to determine integrated gas-phase metallicities, normalised for direct comparison as per the prescriptions of Kewley & Ellison (2008). Boselli et al. (2014) present 21 cm atomic hydrogen observations and $^{12}\text{C}^{16}\text{O}(1-0)$ molecular gas observations. We note that most of the CO observations in Boselli et al. (2014) are single-dish central pointings, with only partial coverage of the target galaxies (they infer the total CO emission assuming exponential molecular gas discs); they do, however, present and homogenise literature CO observations that fully map HRS galaxies.

To use Equation 10, we need FIR-submm photometry (with which to fit the dust SED), 21 cm measurements, $^{12}\text{C}^{16}\text{O}(1-0)$ measurements, and gas-phase metallicities – all integrated over the entire target galaxy. In total, 22 HRS galaxies have this complete range of data available; these are the galaxies we use in Section 5 when determining the value of κ_d . These 22 galaxies span a stellar mass range of $10^{9.7} < M_* < 10^{11.0} M_\odot$, and a metallicity range of $8.61 < [12 + \log_{10} \frac{O}{H}] < 8.86$.

This dataset represents an enormous improvement over what was available to James et al. for their original determination of κ_d . In particular, the *Herschel* photometry of the HRS galaxies allows for far better SED fitting than was possible with the IRAS⁸ 12–100 μm and JCMT SCUBA⁹ 850 μm data that James et al. had at their disposal. Similarly, the metallicities used by James et al. were not integrated measurements of the kind available for the HRS, but instead were derived from observations of a few individual HII regions only, and pre-date the metallicity-normalisation procedure of Kewley & Ellison (2008).

The basic properties of the galaxies in our sample are given in Table B1, and the gas masses and metallicities are given in Table B3

4 SED FITTING

We opt to use 500 μm as our reference wavelength for determining κ_d , as it is a common choice in the literature (allowing for easy comparison), and because it is the longest *Herschel* wavelength, and hence the least affected by dust temperature.

For each source, we determine S_{500c} , S_{500w} , T_c , and

T_w , by fitting a two-component modified blackbody model to the dust SED from 60–500 μm , using a χ^2 -minimising routine which incorporates the colour-corrections for filter response function and beam area^{10,11,12,13}. Note that for a galaxy with an SED that is well-fit by a single-component model, this method is free to assign negligible mass to one of the dust components, or fit two identical-temperature components. We use the 100, 160, 250, 350, and 500 μm fluxes published by the HRS¹⁴, whilst at 60 μm we use IRAS photometry obtained using the Scan Processing and Integration Tool (SCANPI¹⁵), following the procedure laid out by Sanders et al. (2003). Note that this photometry is all at sufficiently long wavelengths that it will be unaffected by Polycyclic Aromatic Hydrocarbon (PAH) emission, which occurs at wavelengths $\lesssim 20 \mu\text{m}$ (Draine & Li, 2007; da Cunha et al., 2008). We also use the 22 μm fluxes published by the HRS as upper limits, to prevent unconstrained warm components from being fitted.

When modelling FIR-submm SEDs, there is a well-established degeneracy between temperature and β (Shetty et al., 2009; Smith et al., 2013), that leads to an artificial anticorrelation. To confuse matters further, methods that should be ‘immune’ to the temperature- β degeneracy give conflicting results regarding the actual variation of β with temperature; the hierarchical Bayesian fitting approach of Kelly et al. (2012) indicates that temperature and β are positively correlated, whilst the laboratory analysis of Demyk et al. (2013) suggests that there is in fact a real, underlying temperature- β anticorrelation. For these reasons, we opt to employ a fixed β in this work; specifically, we use a value of $\beta = 2$, as both observational (Dunne & Eales, 2001; Clemens et al., 2013; Smith et al., 2013; Planck Collaboration et al., 2014b) and experimental (Demyk et al., 2013) evidence suggests that values in the range 1.8–2.0 are appropriate for nearby galaxies. Recent work has shown that when keeping β fixed, a single-component modified blackbody SED can systematically fail to fit the dust emission of galaxies (particularly in the case of late types), whilst a two-component model works well (Clark et al., 2015); hence this is the model we use (moreover, Rémy-Ruyer et al., 2015 have shown that the single-component modified blackbody approach can systematically fail even when β is left free to vary). Fixing β does, however, artificially reduce the uncertainty in SED fits; we address this in Section 5.1.

The SEDs are shown in Figure B1. The best-fit values for each parameter are given in Table B2.

³ Spectral and Photometric Imaging REceiver (Griffin et al., 2010)

⁴ Photodetector Array Camera and Spectrometer (Poglitsch et al., 2010)

⁵ Wide-field Infrared Survey Explorer (Wright et al., 2010)

⁶ Sloan Digital Sky Survey (York et al., 2000)

⁷ GAlaxy Evolution EXplorer (Morrissey et al., 2007)

⁸ InfraRed Astronomical Satellite (Neugebauer et al., 1984)

⁹ James Clerk Maxwell Telescope Submillimetre Common-User Bolometer Array (Holland et al., 1999)

¹⁰ SPIRE handbook: http://herschel.esac.esa.int/Docs/SPIRE/spire_handbook.pdf.

¹¹ PACS instrument and calibration wiki: <http://herschel.esac.esa.int/twiki/bin/view/Public/PacsCalibrationWeb>.

¹² IRAS LAMBDA explanatory supplement: <http://lambda.gsfc.nasa.gov/product/iras/>

¹³ WISE all-sky data release explanatory supplement: <http://wise2.ipac.caltech.edu/docs/release/allsky/expsup/>.

¹⁴ We corrected the HRS fluxes to account for a recently-fixed error in the Scanamorphos pipeline (Roussel, 2013) used to create the HRS PACS maps. The published HRS fluxes at 100 and 160 μm were multiplied by 1.01 and 0.93 respectively, the average change (with scatter ~ 2 per cent) in extended-source flux in maps produced with corrected versions of Scanamorphos.

¹⁵ <http://irsa.ipac.caltech.edu/applications/Scanpi/>

Table 1. Values and uncertainties of κ_{500} determined for the galaxies of our sample, and the sample as a whole. The \pm uncertainties on each value are asymmetric, and are defined by the 66.6th percentiles away from the determined value along the bootstrapped distributions (in each direction). We also quote approximately-equivalent logarithmic uncertainties (in dex), defined by the 66.6th percentile away from the determined values in absolute terms (ie, in both directions). The overall sample value of κ_{500} is the median value.

Name	κ_{500}	$-\kappa_{500}$	$+\kappa_{500}$	$\Delta \kappa_{500}$
	(m ² kg ⁻¹)			(dex)
NGC 3437	0.048	-0.039	+0.078	0.157
NGC 3631	0.042	-0.029	+0.118	0.252
NGC 3683	0.055	-0.043	+0.147	0.310
NGC 3953	0.064	-0.045	+0.186	0.285
NGC 4030	0.055	-0.045	+0.125	0.272
M 98	0.063	-0.051	+0.119	0.195
NGC 4212	0.059	-0.047	+0.132	0.245
M 99	0.037	-0.030	+0.085	0.248
M 61	0.039	-0.031	+0.079	0.210
M 100	0.067	-0.054	+0.146	0.243
M 86	0.054	-0.043	+0.131	0.283
M 88	0.071	-0.057	+0.163	0.274
NGC 4527	0.042	-0.035	+0.084	0.211
NGC 4535	0.067	-0.055	+0.127	0.203
NGC 4536	0.062	-0.033	+0.154	0.242
NGC 4567	0.014	-0.011	+0.038	0.335
NGC 4568	0.061	-0.042	+0.209	0.356
M 60	0.033	-0.025	+0.092	0.327
NGC 4651	0.042	-0.033	+0.077	0.179
NGC 4654	0.046	-0.037	+0.086	0.194
NGC 4689	0.049	-0.038	+0.139	0.342
NGC 5248	0.042	-0.035	+0.080	0.203
Overall	0.051	-0.026	+0.070	0.244

5 DETERMINING THE DUST MASS ABSORPTION COEFFICIENT

We now have the values necessary to use Equation 10 to determine κ_{500} for each of the galaxies in our sample; the resulting values are listed in Table 1. The values range from $\kappa_{500} = 0.031 \text{ m}^2 \text{ kg}^{-1}$ (for NGC 4567), to $\kappa_{500} = 0.071 \text{ m}^2 \text{ kg}^{-1}$ (for M 88). The median value is $\kappa_{500} = 0.051 \text{ m}^2 \text{ kg}^{-1}$.

5.1 Uncertainties

To determine the uncertainty on the value of κ_{500} for each galaxy in our sample, we employ a Monte Carlo bootstrapping analysis, whereby the parameters in Equations 3, 5, 6, 7, 8, and 10 were re-sampled, and the value of κ_{500} was recalculated; this process was repeated 50,000 times for each source.

We generated re-sampled values of ε_d , S_{HI} , S_{CO} , δ_O , $[12 + \log_{10} \frac{O}{H}]$ (and hence Z), $[\frac{O}{H}]_{\odot}$, f_{He_p} , $[\frac{\Delta f_{He}}{\Delta f_Z}]$, A , N , α_{CO} ¹⁶, T_c , T_w , S_{500_c} , and S_{500_w} . The uncertainties on

¹⁶ A re-sampled value of α_{CO} is dictated by the perturbed values of $[12 + \log_{10} \frac{O}{H}]$, A , and N , as per Equation 8, generated by randomly perturbing each according to a Gaussian distribution defined by their given uncertainties. However, as previously stated, Schrubla et al. (2012) find 0.1 dex of scatter on their prescription

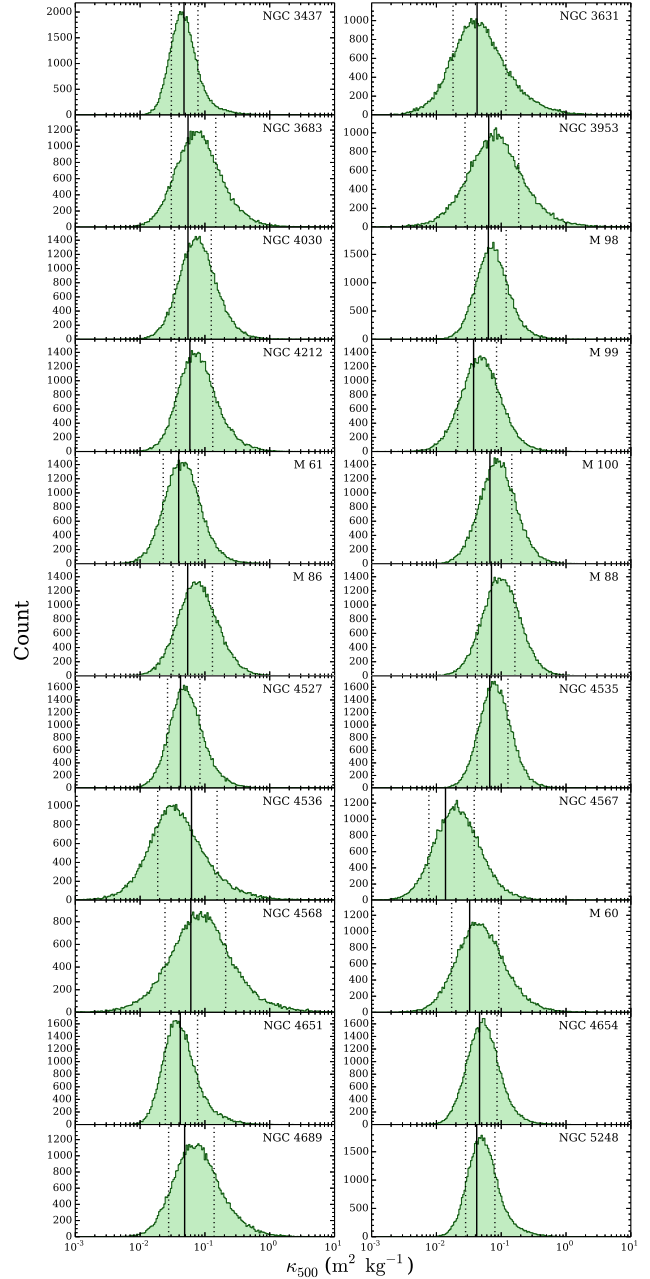


Figure 2. The distributions of values of κ_{500} produced by bootstrapping Equations 3, 5, 6, 7, 8, and 10, for each of the galaxies in our sample. The actual value of κ_{500} determined for each galaxy is indicated by the solid black line. We define the uncertainties on each value by the 66.6th percentiles away from the determined value along the bootstrapped distributions (in each direction); these are indicated by the dotted black lines.

$[12 + \log_{10} \frac{O}{H}]$, α_{CO} , and $[\frac{O}{H}]_{\odot}$ are quoted in dex, and so the perturbations were carried out in logarithmic space; for the other parameters, the uncertainties are stated as simple \pm values, and so the perturbations were carried out in linear

as a whole; we therefore further perturbed each generated value of α_{CO} accordingly.

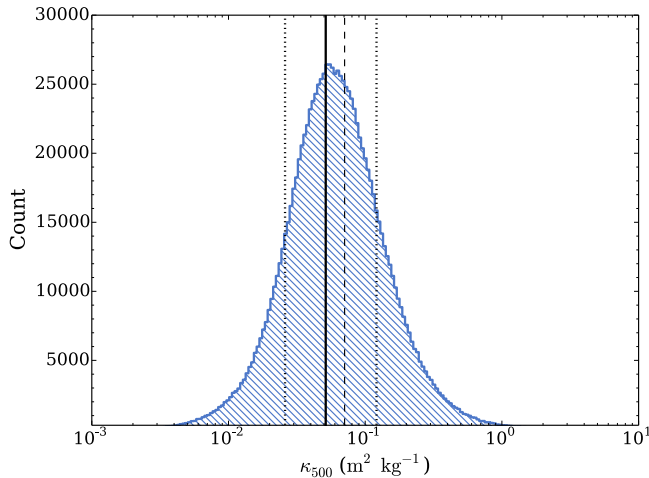


Figure 3. The distribution of values of κ_{500} produced by combining all of the bootstrapped distributions in Figure 2. The median determined value of κ_{500} is indicated by the solid black line. The dotted black lines indicate the uncertainties on this value, defined by the 66.6th percentiles away from the median value along the bootstrapped distribution (in each direction). Also plotted, for comparison, is a dashed black line indicating the alternate value of κ_{500} calculated in Section 5.2, using a constant Milky Way α_{CO} (as opposed to the metallicity-dependant value used for the main determination).

space. The uncertainties on S_{HI} and S_{CO} were taken to be the Root-Mean-Square (RMS) noise values quoted in Boselli et al. (2014). For sources for which Boselli et al. (2014) do not give an RMS noise, we assume a ‘worst-case scenario’ detection with a Signal-to-Noise Ratio (SNR) of 2.

The re-sampled values of T_c , T_w , S_{500c} , and S_{500w} were produced by re-fitting the SED for each bootstrapping iteration; the 22–500 μm fluxes were randomly perturbed according to a Gaussian distribution defined by their uncertainties, and a best fit was then made to this re-sampled SED. Whilst we had used a fixed $\beta = 2$ when carrying out the SED fits to the actual measured fluxes of each source, we left β free when performing the bootstrapping; otherwise our uncertainties would have been artificially small.

The distribution of bootstrapped values of κ_{500} for each galaxy are shown in Figure 2. The distributions are generally asymmetric, and as such we define our uncertainties asymmetrically; specifically, by the 66.6th percentile away from the determined value along the bootstrapped distribution, in each direction. The resulting values are given in Table 1 (also listed for each source is the approximately-equivalent logarithmic uncertainty, in dex, defined by the 66.6th percentile away from the determined value in absolute terms). The median value of $\kappa_{500} = 0.051 \text{ m}^2 \text{ kg}^{-1}$ is in agreement with the values of all of the sources to within their individual uncertainties, with the exception of NGC 4567.

To determine the uncertainty on the average value of κ_{500} , we merged the bootstrapped distributions of all 22 galaxies in our sample; the resulting combined distribution is plotted in Figure 3. We use this distribution to define the uncertainty on the median value of κ_{500} , as before. With these uncertainties, we therefore find a value of the dust mass absorption coefficient κ_d at a wavelength of 500 μm of

$\kappa_{500} = 0.051^{+0.070}_{-0.026} \text{ m}^2 \text{ kg}^{-1}$. The approximately-equivalent logarithmic uncertainty on this value is 0.24 dex.

5.2 Milky Way α_{CO}

For comparison and redundancy, we also determine κ_{500} using molecular gas masses determined using a constant Milky Way CO-to-H₂ conversion factor of $\alpha_{CO} = 3.2 \text{ M}_{\odot}$. This value is considered to be uncertain by a factor of ~ 2 (see review in Saintonge et al., 2011). Using this value of α_{CO} , but otherwise proceeding in the exact same manner as before, gives a κ_d value of $\kappa_{500} = 0.071^{+0.096}_{-0.036} \text{ m}^2 \text{ kg}^{-1}$. This is well within the uncertainty of the value produced using the metallicity-dependant α_{CO} .

6 VARIATION IN κ_d

We now examine whether κ_d correlates with any of the properties of the galaxies in our sample. The properties we consider are: M_{\star} (stellar mass), M_d , M_d/M_{\star} , T_c , L_{TIR} (total infrared luminosity), M_{HI} , M_{H_2} , M_{HI}/M_{\star} , M_{HI}/M_{H_2} , SFR (star formation rate), SFR/M_{\star} , Z , D25 (the angular diameter at the 25th magnitude per square arcsecond isophote), and L_{TIR}/L_{FUV} (a proxy for FUV dust attenuation). The values of M_{\star} , L_{TIR} , SFR , D25 and L_{FUV} are the same as used in Section 5.1.1 of Clark et al. (2015).

In turn, we plotted the κ_{500} values of the galaxies in our sample against each of the parameters in question, and found the best-fit straight line, using a χ^2 -minimisation approach. We then bootstrapped these fits 1000 times each, randomly perturbing the value of κ_{500} for every galaxy, according to the distributions shown in Figure 2. The results are compatible with there being no correlation of κ_{500} with any of the parameters considered. Similarly, for each relationship, Spearman rank correlation tests do not allow us to reject the null hypothesis (of there being no correlation) to a likelihood of < 0.01 . We note, however, that the size of our sample is small compared to the scale of the uncertainties on κ_{500} ; hence we in no way rule out that such correlations could exist, but not be detectable in our data.

7 COMPARISON TO PREVIOUS ESTIMATES

As can be seen in Figure 1, our determined value of κ_d is low compared to existing literature values (although the very commonly-used values of Draine, 2003 and Draine & Li, 2007 are within our bootstrapped uncertainty). Converting the James et al. value to a wavelength of 500 μm for comparison with our own, as per Equation 1, translates it to $\kappa_{500} = 0.20 \pm 0.06 \text{ m}^2 \text{ kg}^{-1}$; a factor of 3.92 larger than our value, despite the fact we employ the same fundamental technique; it is important to address the reasons for this.

As discussed in Section 2, our consideration of systematic effects, using ξ (ie, the contribution of helium and metals to a galaxy’s gas mass) and δ_O (ie, oxygen-depletion in HII regions) will account for a factor 1.86 reduction in κ_d relative to James et al.. We also employ a slightly larger value of ε_d (0.5 versus 0.456), leading to a further factor 1.10 reduction in κ_d . However, our use of a more modern, smaller value of $f_{Z_{\odot}}$ (0.0134 versus 0.019) works in the opposite direction, diminishing the reduction in κ_d by a factor of 0.71. In combination, these global effects correspond to a factor

1.42 reduction in κ_d relative to James et al.; additional effects must be at work to explain the full difference between our values.

Fortunately, M61 (NGC 4303) is present in both the James et al. sample and our own, allowing for a direct comparison of the reasons for the difference in values for a specific case. For M61, we find that our result of $\kappa_{500} = 0.039 \text{ m}^2 \text{ kg}^{-1}$ (see Table 1) is a factor of 5.13 less than the $\kappa_{500} = 0.20 \text{ m}^2 \text{ kg}^{-1}$ value that James et al. found for their sample as a whole. James et al. did not work out values of κ_d for individual sources, but do say that there is scatter of a factor of 2 around their sample-wide relation, hence we need to account for a factor of $5.31^{+5.13}_{-2.57}$ difference between our κ_d for M61, and the James et al. sample-wide value. In Appendix A, we work through each of the sources of difference in our values of κ_d in the case of M61, and find that a factor of 6.31 is to be expected, well within the predicted range – highlighting the dramatic influence of considering systematic effects and utilising superior observations.

During the *Herschel* Science Demonstration Phase, Eales et al. (2010) applied a resolved variant of the James et al. method (where they pegged the dust mass surface density to the gas mass surface density, assuming a fixed Schmidt-Kennicutt law and a Milky Way dust-to-gas ratio) to observations of two of the first HRS targets, M99 and M100. Whilst their analysis was limited by the fact they had *Herschel* observations of only these two galaxies, and assumed an uncorrected solar metallicity, they noted that once the HRS was complete it would represent an ideal dataset for a full determination of κ_d . Converted to our $500 \mu\text{m}$ reference wavelength as per Equation 1, they found $\kappa_{500} = 0.027 \text{ m}^2 \text{ kg}^{-1}$ for M99, and $\kappa_{500} = 0.031 \text{ m}^2 \text{ kg}^{-1}$ for M100. These values are smaller than (although still within the uncertainties of) the values we find for these galaxies; indeed, as seen in Figure 1, these are the smallest of all values of κ_d reported in the literature. The nature of the resolved analysis employed by Eales et al. (2010) makes it difficult to directly compare our values; however, the fact that they could only consider pixels with significant detections of dust, HI, and CO, will have limited their analysis to regions with higher ISM surface-density – regions which might therefore have systematically different dust properties.

In contrast to this, the reader should note that we are using integrated, galaxy-wide values for all of our measurements. This is relevant to the HI component in particular, as it is conceivable that the mass in an extended HI disc may not have a direct bearing upon the properties of the dust and gas found within the inner disc. If so, we would be overestimating the M_{HI} term in Equation 10, and hence finding an artificially small value of κ_d . However, we have reasons to believe that this is unlikely to be significantly distorting our result. The work of Ménard et al. (2010) and Smith et al. (*submitted*) indicate that a significant fraction of a galaxy’s dust mass is found outside the main stellar disc (Ménard et al. infer from quasar reddening that half the dust mass is found beyond the stellar discs of galaxies, whilst Smith et al. perform submm stacking of the HRS galaxies and find that 10% of galaxies’ dust mass lies outside the optical D25, following an exponential profile). This shouldn’t necessarily be surprising, given that the ISM in the outer discs of massive spiral galaxies has been shown to be metal-rich, even out to large optical radii (Werk et al.,

2011; Patterson et al., 2012). Furthermore, Dunne et al. (*in prep.*) show that significant masses of dust can reside in an atomic-gas-dominated medium where there is only a minimal molecular gas component. The HRS submm photometry of Ciesla et al. (2012) used large apertures, with sizes 1.4–3.3 times the optical D25 for the galaxies in our sample; as such, the (likely faint) emission from any extended dust component will be incorporated into the submm fluxes we use. Similarly, given the observing strategy described by (Boselli et al., 2013), the HRS drift-scan spectroscopy sampled the region beyond the optical disc for 82 per cent of the galaxies in our sample; in these cases, the metallicity of the outer disc will hence have been sampled¹⁷ (in a luminosity-weighted manner). Regardless, the galaxies of our sample do not actually appear to possess significantly-extended atomic gas discs. Resolved 21 cm observations are available in the literature for 59 per cent of our sample¹⁸, and for these objects the submm photometric apertures encircle an average of 95 per cent of the detected 21 cm emission (with a minimum of 88 per cent) – whilst the optical D25 isophotes contain an average of 80 per cent of the 21 cm emission. As such, even in the unphysically extreme scenario where the atomic gas beyond the optical D25 contains no dust at all, a value of κ_d determined using our method would be underestimated by no more than a factor of 1.2.

Directly comparing our value for κ_d to those determined via other means is problematic. At the most fundamental level our method is similar to many theoretical approaches, in that the initial consideration is the fraction of metals depleted into dust grains – indeed, our final value of κ_d is compatible with that determined by Draine (2003) and Draine & Li (2007), who work from that very premise. However, beyond this first step, it is very difficult to compare an empirical result such as ours to theoretical values that arise from considerations of astrochemistry and complex Mie theory calculations. Similar calculations go into estimates based upon radiative transfer modelling, which additionally rely upon assumptions about the optical properties and/or geometry of the dust being modelled, making them equally troublesome to compare to. However, whilst these differences make other values for κ_d impractical to compare to our own, we argue that this renders them highly complementary.

8 CONCLUSIONS

We apply the method of James et al. (2002) to the rich, homogeneous dataset of the HRS. This technique enables us to determine the dust mass in a galaxy without needing to use FIR–submm photometry; by relating this calculated dust mass to the observed dust emission, we can empirically find the value of the dust mass absorption coefficient, κ_d .

We find a value of κ_d at a wavelength of $500 \mu\text{m}$ of $\kappa_{500} = 0.051^{+0.070}_{-0.026} \text{ m}^2 \text{ kg}^{-1}$. The uncertainty on this value

¹⁷ For those galaxies, an average of 30 per cent of the solid angle scanned by the spectroscopy was beyond the optical D25.

¹⁸ Resolved 21 cm data measurements from Knapen (1997) for NGC 3631, Verheijen & Sancisi (2001) for NGC 3953, and the VLA Imaging of Virgo spirals in Atomic gas (VIVA, Chung et al., 2009) survey for the rest. Of the galaxies with resolved 21 cm data available, 23 per cent are not associated with the Virgo Cluster; for the sample as a whole, the fraction is 32 per cent.

was determined rigorously, by bootstrapping for every input parameter, taking the uncertainty on the prescriptions employed, and the individual measurements used.

Empirical determinations of κ_d , such as this, provide a vital counterpoint to the development of theoretical dust models, as there are precious few ways in which the properties of dust can be observationally determined.

We note that our value for κ_d is susceptible to an additional systematic offset of up to 0.7 dex, due to the uncertainty in the absolute metallicity scale calibration (Kewley & Ellison, 2008). However, even when the full worst-case offset of 0.7 dex is combined with the results of our bootstrapping analysis, the combined uncertainty of ~ 0.74 dex is *still* less than the generally assumed ‘order-of-magnitude’ uncertainty on κ_d .

With a single exception, the values of κ_d we determine for the galaxies in our sample agree to within their uncertainties. Naïvely speaking, one would expect this to be true for only ~ 66 per cent of the sample. This suggests that the uncertainty values (the majority of which we take from the literature, with the exception of those derived from our SED fits) incorporated into our bootstrapping analysis have, on average, been overestimated by their respective authors.

We find no evidence that κ_d varies as a function of any of the properties of the galaxies in our sample. However, as we opted to limit our sample to HRS galaxies that share the full set of homogeneous integrated measurements required, our sample consists only of relatively massive ($10^{9.7} < M_\star < 10^{11.0} M_\odot$), high metallicity ($8.61 < [12 + \log_{10} \frac{O}{H}] < 8.86$) systems. To truly establish if (and how) the value of κ_d changes between galaxies is vital for the field – despite the huge advances in dust astrophysics over the past 10–15 years, we still have little idea if and how the value of κ_d differs between galaxies. But doing so requires homogeneous high-quality data for a wider range of systems than are available at present.

Fortunately, large Integral Field Unit (IFU) spectroscopy surveys such as CALIFA¹⁹, SAMI²⁰, and MaNGA²¹ mean that integrated metallicity measurements will soon be available for vastly greater numbers of galaxies. Similarly, statistically-large local-Universe CO surveys, such as JINGLE²², are becoming more common. Once these datasets become available, it will be possible to use the method we employ here to constrain the value of κ_d for galaxies with a far broader range of properties.

9 ACKNOWLEDGEMENTS

The authors would like to thank the anonymous referee for their valuable comments, which lead to substantive improvements to this work.

CJRC acknowledges support from the European Research Council (ERC) in the form of the FP7 project DustPedia (PI Jon Davies, proposal 606824) and the Science

and Technology Facilities Council (STFC) Doctoral Training Grant scheme, and kindly thanks Steve Eales and Matt Smith for helpful conversations.

SPS acknowledges support from the STFC Doctoral Training Grant scheme. JID acknowledges support from the ERC in the form of the FP7 project DustPedia (proposal 606824). HLG acknowledges support from the ERC in the form of Consolidator Grant project COSMICDUST (proposal 647939).

This research has made use of Astropy²³, a community-developed core Python package for Astronomy (Astropy Collaboration et al., 2013). This research has made use of TOPCAT²⁴ (Taylor, 2005), which was initially developed under the UK Starlink project, and has since been supported by PPARC, the VOTech project, the AstroGrid project, the AIDA project, the STFC, the GAVO project, the European Space Agency, and the GENIUS project. This research has made use of NumPy²⁵ (Walt et al., 2011), SciPy²⁶, and Matplotlib²⁷ (Hunter, 2007). This research has made use of the SIMBAD²⁸ database (Wenger et al., 2000) and the VizieR²⁹ catalogue access tool (Ochsenbein et al., 2000), both operated at CDS, Strasbourg, France. This research has made use of the NASA/IPAC Infrared Science Archive (IRSA³⁰), operated by the Jet Propulsion Laboratory, California Institute of Technology, under contract with the National Aeronautics and Space Administration. This research has made use of code written by Adam Ginsburg³¹, kindly made available under the GNU General Public License³².

Herschel is an ESA space observatory with science instruments provided by European-led Principal Investigator consortia and with important participation from NASA. The *Herschel* spacecraft was designed, built, tested, and launched under a contract to ESA managed by the *Herschel/Planck* Project team by an industrial consortium under the overall responsibility of the prime contractor Thales Alenia Space (Cannes), and including Astrium (Friedrichshafen) responsible for the payload module and for system testing at spacecraft level, Thales Alenia Space (Turin) responsible for the service module, and Astrium (Toulouse) responsible for the telescope, with in excess of a hundred subcontractors.

References

- Alton P. B., Xilouris E. M., Bianchi S., Davies J., Kylafis N., 2000, *A&A*, 356, 795
- Alton P. B., Xilouris E. M., Misiriotis A., Dasyra K. M., Dumke M., 2004, *A&A*, 425, 109
- Asano R. S., Takeuchi T. T., Hirashita H., Inoue A. K., 2011, in *Astronomical Society of the Pacific Conference Series*, Vol. 445, Why Galaxies Care about AGB Stars II:

¹⁹ Calar Alto Legacy Integral Field spectroscopy Area survey (Sánchez et al., 2012).

²⁰ Sydney-AAO Multi-object Integral-field spectrograph (Bryant et al., 2015).

²¹ Mapping Nearby Galaxies at APO (Bundy et al., 2015).

²² JCMT dust and gas In Nearby Galaxies Legacy Exploration.

²³ <http://www.astropy.org/>

²⁴ <http://www.star.bris.ac.uk/~mbt/topcat/>

²⁵ <http://www.numpy.org/>

²⁶ <http://www.scipy.org/>

²⁷ <http://matplotlib.org/>

²⁸ <http://simbad.u-strasbg.fr/simbad/>

²⁹ <http://vizier.u-strasbg.fr/viz-bin/VizieR>

³⁰ <http://irsa.ipac.caltech.edu/frontpage/>

³¹ <https://github.com/keflavich>

³² <http://www.gnu.org/copyleft/gpl.html>

- Shining Examples and Common Inhabitants, Kerschbaum F., Lebzelter T., Wing R. F., eds., p. 523
- Asplund M., Grevesse N., Sauval A. J., Scott P., 2009, *ARA&A*, 47, 481
- Astropy Collaboration et al., 2013, *A&A*, 558, A33
- Aver E., Olive K. A., Porter R. L., Skillman E. D., 2013, *JCAP*, 11, 17
- Balser D. S., 2006, *AJ*, 132, 2326
- Bianchi S., Gonçalves J., Albrecht M., Caselli P., Chini R., Galli D., Walmsley M., 2003, *A&A*, 399, L43
- Boselli A., Cortese L., Boquien M., 2014, *A&A*, 564, A65
- Boselli A. et al., 2010, *PASP*, 122, 261
- Boselli A., Hughes T. M., Cortese L., Gavazzi G., Buat V., 2013, *A&A*, 550, A114
- Bresolin F., Gieren W., Kudritzki R.-P., Pietrzyński G., Urbaneja M. A., Carraro G., 2009, *ApJ*, 700, 309
- Bryant J. J. et al., 2015, *MNRAS*, 447, 2857
- Bundy K. et al., 2015, *ApJ*, 798, 7
- Cardelli J. A., Meyer D. M., Jura M., Savage B. D., 1996, *ApJ*, 467, 334
- Casey S. C., 1991, *ApJ*, 371, 183
- Chen B., Dai X., Kochanek C. S., Chartas G., 2013, *arXiv:1306.0008*
- Chung A., van Gorkom J. H., Kenney J. D. P., Crowl H., Vollmer B., 2009, *AJ*, 138, 1741
- Ciesla L. et al., 2014, *A&A*, 565, A128
- Ciesla L. et al., 2012, *A&A*, 543, A161
- Clark C. J. R. et al., 2015, *MNRAS*, 452, 397
- Clemens M. S. et al., 2013, *MNRAS*, 433, 695
- Compiègne M. et al., 2011, *A&A*, 525, A103
- Corbelli E. et al., 2012, *A&A*, 542, A32
- Cortese L. et al., 2012a, *A&A*, 544, A101
- Cortese L. et al., 2012b, *A&A*, 540, A52
- Cortese L. et al., 2014, *MNRAS*, 440, 942
- da Cunha E., Charlot S., Elbaz D., 2008, *MNRAS*, 388, 1595
- Dasyra K. M., Xilouris E. M., Misiriotis A., Kylafis N. D., 2005, *A&A*, 437, 447
- Davies J. I. et al., 2014, *MNRAS*, 438, 1922
- Demyk K. et al., 2013, in *Proceedings of The Life Cycle of Dust in the Universe: Observations, Theory, and Laboratory Experiments (LCDU2013)*. 18-22 November, 2013. Taipei, Taiwan. Editors: Anja Andersen, Maarten Baes, Haley Gomez, Ciska Kemper, Darach Watson.
- Draine B. T., 2003, *ARA&A*, 41, 241
- Draine B. T. et al., 2007, *ApJ*, 663, 866
- Draine B. T., Lee H. M., 1984, *ApJ*, 285, 89
- Draine B. T., Li A., 2007, *ApJ*, 657, 810
- Dunne L., Eales S., Edmunds M., Ivison R., Alexander P., Clements D. L., 2000, *MNRAS*, 315, 115
- Dunne L., Eales S. A., 2001, *MNRAS*, 327, 697
- Dwek E., 1998, *ApJ*, 501, 643
- Eales S. et al., 2012, *ApJ*, 761, 168
- Eales S. A. et al., 2010, *A&A*, 518, L62
- Gall C. et al., 2014, *Nature*, 511, 326
- Galliano F., Madden S. C., Jones A. P., Wilson C. D., Bernard J.-P., 2005, *A&A*, 434, 867
- Genzel R. et al., 2012, *ApJ*, 746, 69
- Giovanelli R. et al., 2005, *AJ*, 130, 2598
- Griffin M. J. et al., 2010, *A&A*, 518, L3
- Haynes M. P. et al., 2011, *AJ*, 142, 170
- Henry R. B. C., Pagel B. E. J., Lassetter D. F., Chincarini G. L., 1992, *MNRAS*, 258, 321
- Hildebrand R. H., 1983, *QJRAS*, 24, 267
- Holland W. S. et al., 1999, *MNRAS*, 303, 659
- Hughes T. M., Cortese L., Boselli A., Gavazzi G., Davies J. I., 2013, *A&A*, 550, A115
- Hunt L., Bianchi S., Maiolino R., 2005, *A&A*, 434, 849
- Hunter J. D., 2007, *Computing In Science & Engineering*, 9, 90
- Inoue A. K., 2003, *PASJ*, 55, 901
- Issa M. R., MacLaren I., Wolfendale A. W., 1990, *A&A*, 236, 237
- James A., Dunne L., Eales S., Edmunds M. G., 2002, *MNRAS*, 335, 753
- Jenkins E. B., 2009, *ApJ*, 700, 1299
- Jones A., 2013, in *Proceedings of The Life Cycle of Dust in the Universe: Observations, Theory, and Laboratory Experiments (LCDU2013)*. 18-22 November, 2013. Taipei, Taiwan. Editors: Anja Andersen, Maarten Baes, Haley Gomez, Ciska Kemper, Darach Watson.
- Jones A. P., Fanciullo L., Köhler M., Verstraete L., Guillet V., Bocchio M., Ysard N., 2013, *A&A*, 558, A62
- Jones A. P., Tielens A. G. G. M., Hollenbach D. J., 1996, *ApJ*, 469, 740
- Kelly B. C., Shetty R., Stutz A. M., Kauffmann J., Goodman A. A., Launhardt R., 2012, *ApJ*, 752, 55
- Kenney J. D., Young J. S., 1988, *ApJS*, 66, 261
- Kewley L. J., Ellison S. L., 2008, *ApJ*, 681, 1183
- Kim S.-H., Martin P. G., Hendry P. D., 1994, *ApJ*, 422, 164
- Kimura H., Mann I., Jessberger E. K., 2003, *ApJ*, 582, 846
- Knapen J. H., 1997, *MNRAS*, 286, 403
- Kudritzki R.-P., Urbaneja M. A., Gazak Z., Bresolin F., Przybilla N., Gieren W., Pietrzyński G., 2012, *ApJ*, 747, 15
- Kunth D., Östlin G., 2000, *A&A Rev.*, 10, 1
- Leroy A. K. et al., 2011, *ApJ*, 737, 12
- Luck R. E., Lambert D. L., 1992, *ApJS*, 79, 303
- Magrini L. et al., 2011, *A&A*, 535, A13
- Mattsson L., De Cia A., Andersen A. C., Zafar T., 2014, *MNRAS*, 440, 1562
- Ménard B., Scranton R., Fukugita M., Richards G., 2010, *MNRAS*, 405, 1025
- Mesa-Delgado A., Esteban C., García-Rojas J., Luridiana V., Bautista M., Rodríguez M., López-Martín L., Peimbert M., 2009, *MNRAS*, 395, 855
- Messenger S., Keller L. P., Nguyen A. N., 2013, in *Proceedings of The Life Cycle of Dust in the Universe: Observations, Theory, and Laboratory Experiments (LCDU2013)*. 18-22 November, 2013. Taipei, Taiwan. Editors: Anja Andersen, Maarten Baes, Haley Gomez, Ciska Kemper, Darach Watson., p. 40
- Meyer D. M., Jura M., Cardelli J. A., 1998, *ApJ*, 493, 222
- Morrissey P. et al., 2007, *ApJS*, 173, 682
- Mutschke H., 2013, in *Proceedings of The Life Cycle of Dust in the Universe: Observations, Theory, and Laboratory Experiments (LCDU2013)*. 18-22 November, 2013. Taipei, Taiwan. Editors: Anja Andersen, Maarten Baes, Haley Gomez, Ciska Kemper, Darach Watson., p. 42
- Neugebauer G. et al., 1984, *ApJ*, 278, L1
- Ochsenbein F., Bauer P., Marcout J., 2000, *A&AS*, 143, 23
- Patterson M. T., Walterbos R. A. M., Kennicutt R. C.,

Chiappini C., Thilker D. A., 2012, MNRAS, 422, 401
 Pei Y. C., 1992, ApJ, 395, 130
 Pei Y. C., Fall S. M., Hauser M. G., 1999, ApJ, 522, 604
 Peimbert A., Peimbert M., 2010, ApJ, 724, 791
 Pilbratt G. L. et al., 2010, A&A, 518, L1
 Planck Collaboration et al., 2014a, A&A, 571, A11
 Planck Collaboration et al., 2014b, A&A, 564, A45
 Planck Collaboration et al., 2011, A&A, 536, A1
 Poglitsch A. et al., 2010, A&A, 518, L2
 Popping A., Braun R., 2011a, A&A, 533, A122
 Popping A., Braun R., 2011b, A&A, 528, A28
 Rémy-Ruyer A. et al., 2015, arXiv:1507.05432
 Roussel H., 2013, PASP, 125, 1126
 Saintonge A. et al., 2011, MNRAS, 415, 32
 Sánchez S. F. et al., 2012, A&A, 538, A8
 Sanders D. B., Mazzarella J. M., Kim D.-C., Surace J. A.,
 Soifer B. T., 2003, AJ, 126, 1607
 Savage B. D., Sembach K. R., 1996, ApJ, 470, 893
 Schrubba A. et al., 2012, AJ, 143, 138
 Scoville N. et al., 2014, ApJ, 783, 84
 Shetty R., Kauffmann J., Schnee S., Goodman A. A., 2009,
 ApJ, 696, 676
 Shields G. A., Skillman E. D., Kennicutt, Jr. R. C., 1991,
 ApJ, 371, 82
 Skillman E. D., Kennicutt, Jr. R. C., Shields G. A., Zarit-
 sky D., 1996, ApJ, 462, 147
 Smith D. J. B. et al., 2012a, MNRAS, 427, 703
 Smith D. J. B. et al., 2013, MNRAS, 436, 2435
 Smith M. W. L. et al., 2012b, ApJ, 756, 40
 Sodroski T. J., Odegard N., Arendt R. G., Dwek E., Wei-
 land J. L., Hauser M. G., Kelsall T., 1997, ApJ, 480, 173
 Sparre M. et al., 2014, ApJ, 785, 150
 Taylor M. B., 2005, in Astronomical Society of the Pacific
 Conference Series, Vol. 347, Astronomical Data Analysis
 Software and Systems XIV, Shopbell P., Britton M., Ebert
 R., eds., p. 29
 Verheijen M. A. W., Sancisi R., 2001, A&A, 370, 765
 Walt S. v. d., Colbert S. C., Varoquaux G., 2011, Comput-
 ing in Science & Engineering, 13
 Watson D., 2011, A&A, 533, A16
 Weingartner J. C., Draine B. T., 2001, ApJ, 548, 296
 Wenger M. et al., 2000, A&AS, 143, 9
 Werk J. K., Putman M. E., Meurer G. R., Santiago-
 Figueroa N., 2011, ApJ, 735, 71
 Werner M. W. et al., 2004, ApJS, 154, 1
 Whittet D. C. B., 1992, Dust in the galactic environment
 Wright E. L. et al., 2010, AJ, 140, 1868
 York D. G. et al., 2000, AJ, 120, 1579
 Young J. S. et al., 1995, ApJS, 98, 219
 Zafar T., Watson D., 2013, A&A, 560, A26
 Zaritsky D., Kennicutt, Jr. R. C., Huchra J. P., 1994, ApJ,
 420, 87
 Zurita A., Bresolin F., 2012, MNRAS, 427, 1463

A DEVIATION FROM JAMES ET AL. IN THE CASE OF M61

As described in Sections 2 and 7, we find that our calculated values of κ_d should be expected to be smaller than those of James et al. by a factor of 1.42, due to global effects. Here we describe in detail the further differences that should be expected to arise in the useful case of M61, which is in both our sample, and that of James et al..

Whereas James et al. quote a metallicity of $[12 + \log_{10} \frac{O}{H}] = 9.01$ for M61, taken from spectra of individual HII regions³³, we use a metallicity of $[12 + \log_{10} \frac{O}{H}] = 8.67$, derived from integrated drift-scan spectroscopy (Hughes et al., 2013; Boselli et al., 2013) – which should therefore be the superior measurement. This difference in metallicity contributes a further factor 2.19 to the reduction in our value in κ_d relative to that of James et al.. However, the difference in metallicity also gives us a smaller α_{CO} , and hence gas mass, by a factor of 0.71.

James et al. used a lower value of S_{CO} for M61 than we do. Their value is derived from a series of 7 pointings³⁴ along the major axis of M61, extrapolated to the rest of the disc (rendering them unable to account for azimuthal variation) – whereas the value of S_{CO} we take from Boselli et al. (2014) is derived from a mapping of all detected CO emission, with no reliance upon extrapolation, and so is presumably a far more accurate value.

James et al. also quoted a much smaller HI mass for M61 than the one we take from Boselli et al. (2014), leading to an additional factor 2.19 difference in our expected value of κ_d . Unfortunately we are unable to definitively address the underlying reasons for this discrepancy, as James et al. do not seem to provide a reference for the HI mass they use. We note however their HI mass is the same as that given by Magrini et al., 2011, who integrated over the HI radial profile produced by Skillman et al., 1996 out to 0.7 optical radii (due to signal-to-noise constraints in their ancillary data). However, it is unclear if James et al. intentionally chose an HI value that only extends out to some fraction of the optical radius of M61, as most of the HI masses employed by James et al. are those compiled by the SCUBA Local Universe Galaxy Survey (SLUGS, Dunne et al., 2000), whose 21 cm values are point-source integrated measurements taken from the literature. The HI mass we take from Boselli et al. (2014) comes from the 84.71 Jy flux measured by the ALFALFA survey (Arecibo Legacy Fast ALFA, Giovanelli et al., 2005; Haynes et al., 2011), which is in excellent agreement with the 85.2 Jy flux measured at the Westerbork Synthesis Radio Telescope by Popping & Braun (2011b), and the 85.1 Jy flux measured at the Parkes Radio Telescope by Popping & Braun (2011a). As such, it seems that the measurement we use is accurate; possibly simply a benefit of more modern observations.

M61 also illustrates the effect that superior data from *Herschel* has on SED-fitting. The ~ 0.9 order-of-magnitude gap in wavelength coverage suffered by James et al. between the IRAS 100 μm and SCUBA 850 μm points means that

³³ Spectra taken by Shields et al. (1991) and Henry et al. (1992), and compiled by Zaritsky et al. (1994).

³⁴ Observations made by Kenney & Young (1988), and compiled by Young et al. (1995)

they had no coverage of the dust emission peak, making it difficult to constrain dust temperatures. As a result they fixed the temperature of their cold dust component to 20 K when performing their SED fitting. The general shapes of their SED fits are very different from our own (compare their Figure 2 to our Figure B1), with a much more prominent warm component, clearly incompatible with the *Herschel* photometry. Whereas they find that M61 has a cold-to-warm dust mass ratio of $M_c/M_w = 83$ (see their Table 2), we find $M_c/M_w = 7,500$ (their sample median cold-to-warm dust mass ratio is only 19, compared to our median of 2,310). In the case of M61, the net effect is an increase in the value of the section of Equation 10 that incorporates the SED parameters³⁵, which decreases by a factor of 0.87 the expected deviation between our value of κ_d and that of [James et al.](#).

Combining all of these effects leads us to expect our value of κ_d for M61 should be a factor of 6.31 smaller than that of [James et al.](#) (a factor of 1.41 from ξ , 1.32 from δ_O , 1.10 from ε_d , 0.71 from $f_{Z\odot}$, 2.19 from M_{HI} , 1.47 from S_{CO} , 2.19 from Z , 0.71 from α_{CO} , and 0.87 from SED-fitting). The individual effects contributing to the overall difference are all attributable to our consideration of systematic effects, or our use of superior observational measurements (for HI, CO, metallicity, and FIR-submm data).

B PROPERTIES OF THE SAMPLE GALAXIES

Here we present plots and tables detailing the properties of the galaxies in our sample.

³⁵ Specifically, the term: $\left(\frac{S_{\lambda_w}}{B_{\lambda}(T_w)} + \frac{S_{\lambda_c}}{B_{\lambda}(T_c)} \right)$.

Table B1. Basic properties of the HRS galaxies that we study in this work. Values taken from Boselli et al. (2010) and Cortese et al. (2012b).

Name	RA (J2000 deg)	Dec (J2000 deg)	Distance (Mpc)	Heliocentric Velocity (km s ⁻¹)	Morphology (Hubble stage)	Stellar Mass (log ₁₀ M _⊙)
NGC 3437	163.149	22.934	18.2	1277	7	9.69
NGC 3631	170.262	53.170	16.5	1155	7	9.92
NGC 3683	171.883	56.877	24.4	1708	7	10.20
NGC 3953	178.454	52.327	15.0	1050	6	10.60
NGC 4030	180.098	-1.100	20.8	1458	6	10.54
M 98	183.451	14.900	17.0	-135	4	10.65
NGC 4212	183.914	13.902	17.0	-83	7	10.01
M 99	184.707	14.416	17.0	2405	7	10.39
M 61	185.479	4.474	17.0	1568	6	10.51
M 100	185.729	15.822	17.0	1575	6	10.71
M 86	186.531	13.113	17.0	234	5	10.04
M 88	187.997	14.420	17.0	2284	5	10.98
NGC 4527	188.535	2.654	17.0	1736	6	10.67
NGC 4535	188.585	8.198	17.0	1962	7	10.45
NGC 4536	188.613	2.188	17.0	1807	6	10.26
NGC 4567	189.136	11.258	17.0	2277	6	9.92
NGC 4568	189.143	11.239	17.0	2255	6	10.33
M 60	190.885	11.583	17.0	1422	7	10.19
NGC 4651	190.928	16.393	17.0	797	7	10.13
NGC 4654	190.986	13.127	17.0	1039	8	10.14
NGC 4689	191.940	13.763	17.0	1620	6	10.19
NGC 5248	204.384	8.885	16.5	1152	6	10.43

Table B2. Dust properties of the HRS galaxies that we study in this work. The temperatures and 500 μ m fluxes of the cold and warm dust components were determined by fitting a two-component modified blackbody SED to the published HRS photometry, as detailed in Section 4. Note that the quoted uncertainties are merely representative; when bootstrapping to find the total uncertainty in κ_d , we re-fit a bootstrapped SED for every iteration (as described in Section 5).

Name	T_c	ΔT_c	T_w	ΔT_w	S_{500_c}	ΔS_{500_c}	S_{500_w}	ΔS_{500_w}
	(K)				(Jy)	(dex)	(mJy)	(dex)
NGC 3437	23.26	4.15	50.60	15.95	1.25	0.17	27.44	1.28
NGC 3631	20.43	4.27	35.50	19.05	3.17	0.33	74.84	1.69
NGC 3683	24.16	3.47	63.47	14.29	1.53	0.21	9.73	0.99
NGC 3953	18.92	1.47	46.18	18.98	5.09	0.50	5.56	1.58
NGC 4030	21.83	2.41	68.45	17.33	5.01	0.36	8.38	1.41
M 98	19.01	1.82	41.91	18.18	4.72	0.29	25.75	1.34
NGC 4212	21.65	3.70	66.46	18.19	1.78	0.25	4.29	1.19
M 99	22.44	1.43	72.43	17.75	8.68	0.35	3.12	1.78
M 61	22.48	1.64	68.54	17.35	8.09	0.35	5.36	2.06
M 100	20.76	1.33	59.21	18.53	9.74	0.49	3.55	1.91
M 86	20.82	2.42	67.53	16.96	2.01	0.31	3.18	1.10
M 88	20.65	1.48	58.84	18.42	8.46	0.47	6.29	1.62
NGC 4527	21.52	3.04	59.97	18.04	6.75	0.30	29.84	1.23
NGC 4535	19.25	1.79	51.09	19.24	5.88	0.45	11.66	1.60
NGC 4536	17.93	5.18	31.89	18.10	3.96	0.21	924.81	1.24
NGC 4567	19.66	1.68	50.84	2.51	1.32	0.07	41.26	0.25
NGC 4568	22.50	3.78	72.36	15.43	3.81	0.30	4.26	1.15
M 60	21.49	3.06	67.50	17.01	1.61	0.26	3.16	1.07
NGC 4651	18.44	3.96	27.64	19.05	1.79	0.29	337.32	1.57
NGC 4654	20.60	2.16	41.77	17.38	4.48	0.35	57.69	1.48
NGC 4689	19.88	4.27	54.47	17.39	1.73	0.36	2.29	1.63
NGC 5248	21.10	2.21	53.23	17.64	5.89	0.33	27.66	1.43

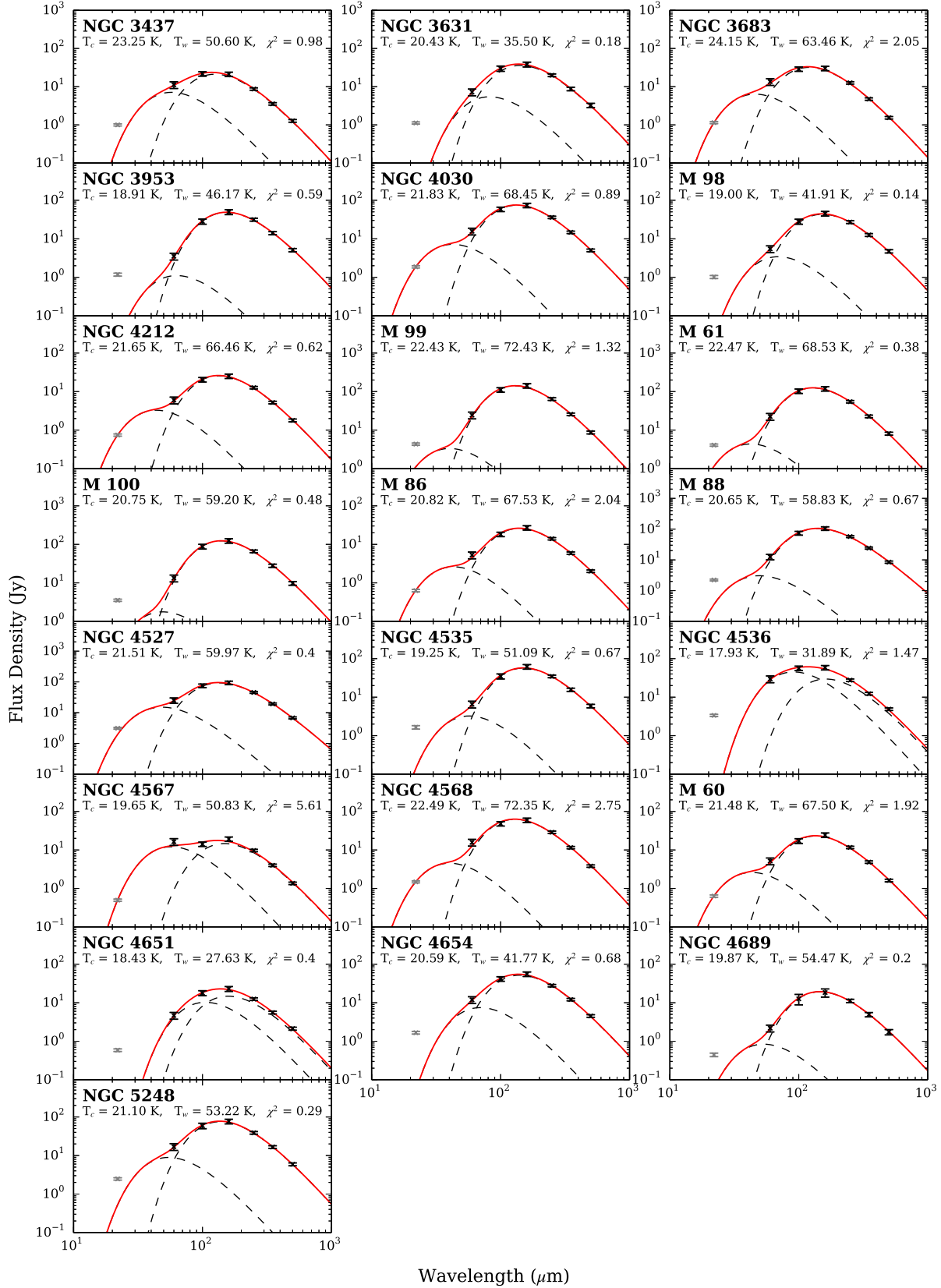


Figure B1. Best-fit FIR-submm SEDs of the galaxies in our sample. The two-temperature modified blackbody fits are shown in red, with the contributions from the warm and cold dust components shown by the dashed curves. The grey $22 \mu\text{m}$ point was treated as an upper limit.

Table B3. Gas properties of the HRS galaxies that we study in this work. HI and CO measurements taken from [Boselli et al. \(2014\)](#). Gas-phase metallicity values taken from [Hughes et al. \(2013\)](#), which used the spectra of [Boselli et al. \(2013\)](#). Note that the metallicities given in the Z column have been corrected for gas-phase oxygen depletion by a factor of $\delta_O = 1.32$, as per Equation 3; as a result, they represent ISM metallicities, not gas-phase metallicities.

Name	S_{HI}	ΔS_{HI}	S_{CO}	ΔS_{CO}	$[12 + \log_{10} \frac{O}{H}]$	$\Delta [12 + \log_{10} \frac{O}{H}]$	Z	α_{CO}
	(Jy km s ⁻¹)					(dex)	(Z_{\odot})	(M _⊙ K ⁻¹ km ⁻¹ s pc ⁻²)
NGC 3437	22.24	2.86	190.00	90.30	8.67	0.03	1.26	9.19
NGC 3631	50.70	25.35 ^a	1093.00	131.40	8.64	0.17	1.18	10.55
NGC 3683	8.27	3.06	390.00	185.30	8.67	0.10	1.26	9.19
NGC 3953	47.79	10.28	1790.00	850.30	8.86	0.22	1.95	3.83
NGC 4030	64.15	5.77	1050.00	498.80	8.69	0.10	1.32	8.38
M 98	74.14	2.25	940.00	446.50	8.76	0.10	1.55	6.07
NGC 4212	13.92	2.20	491.80	59.10	8.71	0.10	1.38	7.64
M 99	77.05	2.42	4033.00	484.80	8.73	0.12	1.45	6.97
M 61	84.71	3.14	3344.00	402.00	8.76	0.11	1.55	6.07
M 100	48.86	2.90	3148.00	378.40	8.75	0.10	1.52	6.35
M 86	7.73	2.62	786.90	94.60	8.68	0.10	1.29	8.77
M 88	29.10	2.28	2951.00	354.70	8.77	0.10	1.59	5.80
NGC 4527	108.50	6.50	1862.00	768.70	8.81	0.10	1.74	4.82
NGC 4535	71.66	2.96	1377.00	165.50	8.77	0.10	1.59	5.80
NGC 4536	74.90	15.00	1082.00	130.10	8.70	0.21	1.35	8.00
NGC 4567	15.64	0.36	2229.00	920.30	8.65	0.10	1.20	10.07
NGC 4568	25.11	0.36	1050.00	498.80	8.77	0.22	1.59	5.80
M 60	7.86	2.94	881.20	363.80	8.61	0.10	1.10	12.11
NGC 4651	62.99	15.24	350.00	166.30	8.75	0.07	1.52	6.35
NGC 4654	50.59	2.52	1574.00	189.20	8.65	0.07	1.20	10.07
NGC 4689	8.36	2.09	786.90	94.60	8.66	0.10	1.23	9.62
NGC 5248	73.58	3.09	2425.00	291.50	8.81	0.06	1.74	4.82

^a [Boselli et al. \(2014\)](#) do not quote an RMS value for the 21 cm flux measurement of NGC 3631; for this source, we assume a ‘worst-case scenario’ detection with SNR = 2.